Gap-Coupled Dual-Band Evanescent-Mode Substrate Integrated Band-Pass Filter Waveguide

Amir Nosrati[1], Mahmud Mohammad-Taheri[1, *], and Mehdi Nosrati[2]

Abstract—A single-layer substrate integrated waveguide (SIW) is developed to design a dual-band band-pass filter (BPF) operating below the cut-off frequency of the SIW, known as evanescent-mode excitation. Gap-coupled excitation is used to demonstrate the multiple transmission poles (TPs) and transmission zeros (TZs) below the cut-off frequency of the SIW. The structure is reported to realize two independent evanescent-mode poles on a single-layer SIW which reduces the size and complexity of the structure compared to those of the recent multi-layer evanescent-mode structures. Lumped-element equivalent circuit is employed to describe the EM behavior of the structure for TZs and TPs realization. A compact single-layer dual-band SIW filter is fabricated based on the proposed structure. A good agreement is reported between the measured and simulated performances.

1. INTRODUCTION

Microwave and millimeter-wave components with reduced complexity and enhanced performance are highly demanded for the new generation of wireless technology such as 5G systems [1]. Reduced complexity mainly includes the planar structures compared to 3D bulky waveguides, single-layer SIW structures in contrast to multi-layer ones, etc. On the other hand, other requirements are the enhanced performances of multi-band devices with high-quality factors and independent tuning of the multi-bands over a wide range of frequencies [2–4]. Evanescent-mode excitation is a promising technique to reduce the size of high-quality 3D structures which employs the unused relatively large frequency range below the cut-off frequency of the waveguide structures. This technique frequently utilizes in BPF's devices through implemented discontinuities between input/output ports for realizing the TPs below a 3D structure's cut-off frequency in which the corresponding device operates in a fraction size of the wavelength. Ordinary mode 3D cavity resonators have a size equal to half of the wavelength, while the evanescent-mode excited structures not only have a smaller size than that of the ordinary mode ones but also show a higher quality-factor. There are different approaches to realize evanescent TPs, e.g., embedded capacitive-plates inside a 3D's structure which can be modeled with a lumped-element LC circuit [5–9]. However, few research studies are reported on the design of multi-band evanescent-mode BPFs [7–9]. While they provide effective techniques, the proposed structures in these studies suffer from either high complexity [7, 8], multi-layer structure, or low-quality factor [9]. Gap-coupled excitation has been recently proposed to excite single/multi-band evanescent-mode BPFs as an alternative for the inductive aperture-coupled technique in the 3D waveguide counterparts [6–8]. Two evanescent-mode BPFs have been developed by this technique. In the first one, a dual-band evanescent-mode BPF has been designed on a dual-layer SIW [8]. In the second case, a single-band evanescent-mode BPF has been designed on a single-layer SIW where one of the bands has been sacrificed in favor of reduced complexity [6]. Two schematic diagrams of that proposed structure in [6] are given in Fig. 1, where the

[1] School of Electrical and Computer Engineering, University of Tehran, Tehran, Iran. [2] Department of Electrical and Computer Engineering, McGill University, Montreal QCH3A0E9, Canada.
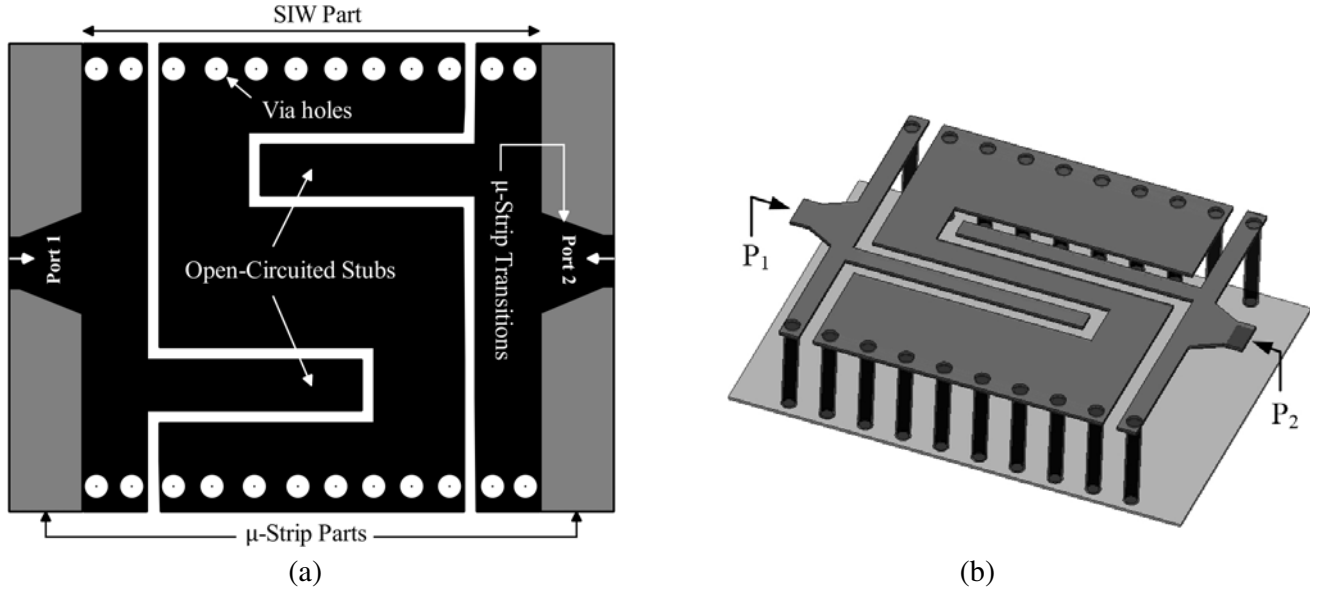
(a)   (b)

Figure 1. (a) 2D and (b) 3D schematic diagrams of the proposed single-band evanescent-mode BPF in [6].

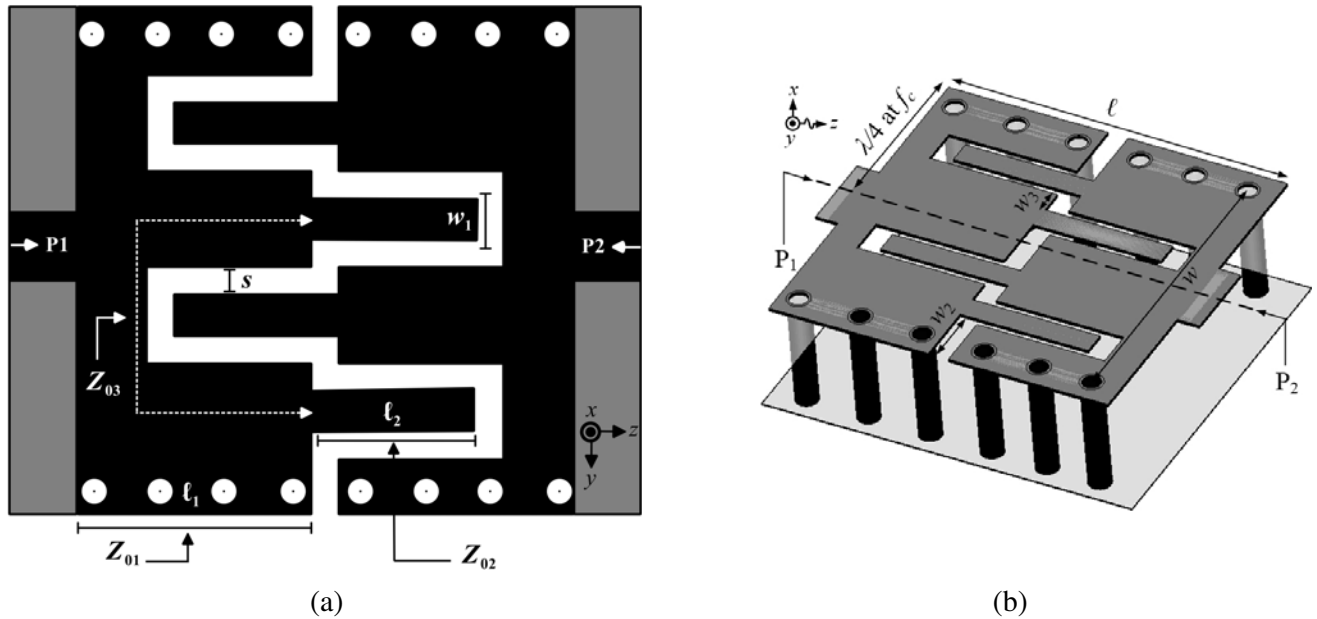(a)   (b)

Figure 2. (a) 2D and (b) 3D schematic diagrams of the developed distributed-element SIW circuit (y-axis and z-axis show the transverse and propagation directions, respectively).

conventional single-band evanescent-mode filter is employed to develop the following dual-band filter. The conventional filter is further developed by adding two extra open-circuited stubs as can be seen in Fig. 2. The extra stubs add a degree of freedom to excite another evanescent-mode TP sandwiched by two TZs.

In this research study, the aim is to design a dual-band evanescent-mode BPF on a single-layer SIW to take advantages of reduced complexity and enhanced performance of the two conventional models. In Section 2, the operation principle of the developed capacitively-coupled structure is discussed for multi evanescent-mode poles' realization using lumped-element equivalent circuit for the distributed-element

structure. A dual-band gap-coupled evanescent-mode BPF is presented in Section 3, accompanied by simulated and experimental results.

2. DESCRIPTION OF OPERATION PRINCIPLE OF MULTI-POLE CAPACITIVELY-COUPLED BPF

Capacitively-coupled structure is used to excite evanescent-mode pole in the BPF structures as well as reduce complexity in the fabrication process. It has been shown that this type of coupling structure demonstrates some priorities over the inductive aperture-coupled structures in terms of size reduction, evanescent-mode pole and TZs realization [3]. Here, the coupling mechanism is developed to further reduce complexity and volume size of the structure. Fig. 2 schematically shows the proposed structure in which two SIWs are capacitively-coupled through four open-circuited stubs in the interdigital configuration. The SIWs are modeled with two parallel LC circuits in the transverse direction (L_1-C_1 and L_2-C_2 circuits in the developed lumped-element circuit model) [7]. The coupling between the two SIWs through the open-circuited stubs is modeled with two series LC circuits, in both the propagation (e.g., $L_{p1,2}$-$C_{p1,2}$) and transverse (e.g., $L_{z1,2}$-$C_{z1,2}$) directions [6]. In the developed structure, two extra open-circuited stubs are added to the conventional structure which they are modeled with ABCD branch circuits in the developed lumped-element equivalent circuit as shown in Fig. 3 [6]. The extra open-circuited stubs provide one more capacitively-coupled path between I/O ports and consequently realize another evanescent-mode transmission pole. Fig. 3 shows the lumped-element equivalent circuit of the developed structure. The lumped-element equivalent circuit can model the EM performance of the distributed-element structure over a wide frequency range [7]. The parallel L_1-C_1 and L_2-C_2 circuits predict the cut-off frequency of the SIWs [6]. Consideration of the two-path lumped-element circuit in Fig. 3, each path realizes a transmission pole and zero as the result of their resonance frequencies.
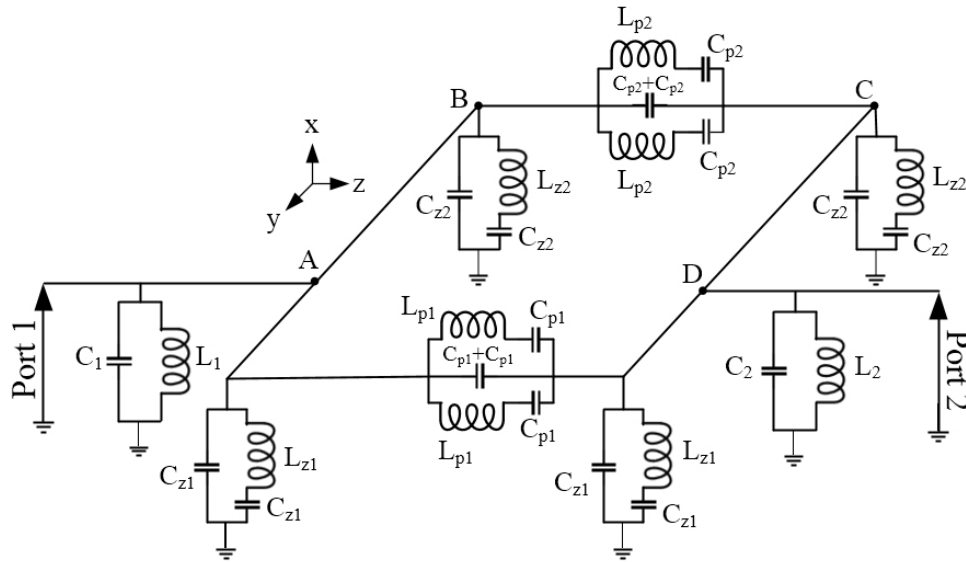

Figure 3. Developed lumped-element equivalent circuit of that distributed SIW circuit given in Fig. 2.

The following equations are employed to determine the values of the lumped-element components [7]:

$$\theta = \lambda/4\,(\beta l = \pi/2) \text{ at } f_c \rightarrow L = Z_0/\pi f_c, \quad C = 1/4\pi Z_0 f_c \tag{1}$$

where θ, Z_0, l, β, and f_c are the electrical length corresponding to the quarter wavelength, characteristic impedance, physical length, phase constant, and cut-off frequency, respectively. From Eq. (2) in [3], the cut-off frequency of the SIW is calculated to be around $f_c = 6.5$ GHz with $w = 13$ mm, $d = 1$ mm and $p = 1.5$ mm, where d and p are the diameter and center to center separation of via holes, respectively.

The structure is simulated on a single-layer Rogers RO4003C substrate with a thickness of 1.524 mm and dielectric constant of 3.55 where Z_0 (for half of the SIW in the propagation direction) is calculated to be 31.5 Ω (microstrip line in the transverse direction with width of $\ell_1 = 7.1$ mm, e.g., Z_{01} given in Fig. 2(a), LineCalc, Agilent ADS). The $0.5C_1$ and $2L_1$ which are capacitor and inductor corresponding to half of the SIW (the length of the SIW corresponding to $\lambda/4$ in the transverse direction) are calculated to be 0.39 pF and 1.54 nH, respectively.

The values of the lumped-element components in the parallel configuration of the two series L_{z1}-C_{z1} and L_{z2}-C_{z2} are calculated using frequencies of TZs. There are two TZs at two distinguished frequencies of $f_{z1} = 4.45$ GHz and $f_{z2} = 6.9$ GHz. Given the $\ell_2 = 6.7$ mm in the transverse direction and $s = 0.3$ mm, the characteristic impedance (e.g., Z_{02} seen in Fig. 2(a)) is calculated to be 46.8 Ω for a coplanar waveguide (CPW). The values of other lumped-element components corresponding to the first and second TZs frequencies are calculated to be $L_{z1} = 3.3$ nH, $C_{z1} = 0.38$ pF and $L_{z2} = 2.15$ nH, $C_{z2} = 0.24$ pF, respectively.

$$w_{eff} = w - 1.08d^2/p + 0.1d^2/w, \quad f_c = C_0/2w_{eff}\sqrt{\varepsilon_r} \tag{2}$$

The series L_{p1}-C_{p1} and L_{p2}-C_{p2} circuits are employed to model the evanescent-mode TPs. The characteristic impedance (e.g., Z_{03} shown in Fig. 2(a)) of the two parallel open-circuited stubs (illustrated by dashed-arrows given in Fig. 2(a)) in the propagation direction is calculated to be $0.5Z_0 = 35\,\Omega$ as a CPW with $w_1 = 1$ mm and $s = 0.3$ mm. Considering the two evanescent-mode TPs at $f_{p1} = 3.5$ GHz and $f_{p2} = 5.4$ GHz, the corresponding L_{p1}, C_{p1} and L_{p2}, C_{p2} components are calculated to be 3.18 nH, 0.65 pF, 2 nH, and 0.42 pF, respectively.

Inspecting the simulation results for the LC model and those of EM in Fig. 4 shows a good agreement that verifies the accuracy of our proposed model and calculations.
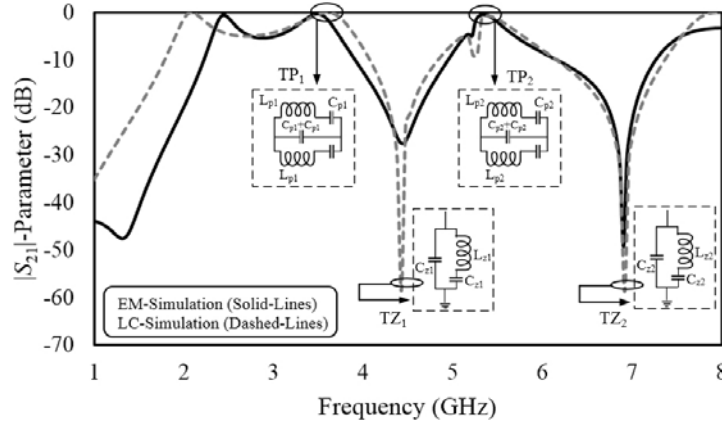

Figure 4. EM- (Method of Moments, Agilent ADS) and LC-simulated S-parameters of the capacitively-coupled structure proposed in Fig. 2 with $\ell = 14.5$, $\ell_1 = 7.1$, $\ell_2 = 6.7$, $w = 13$, $w_1 = 1$, $w_2 = 3.5$, $w_3 = 1.05$, and $s = 0.3$, all in mm for the optimized parameters of the distributed circuit and $C_1 = C_2 = 1.02$ pF, $L_1 = L_2 = 0.61$ nH, $C_{z1} = 0.39$ pF, $L_{z1} = 3.3$ nH, $C_{z2} = 0.24$ pF, $L_{z2} = 2.2$ nH, $C_{p1} = 0.5$ pF, $L_{p1} = 2.39$ nH, $C_{p2} = 0.35$ pF, and $L_{p2} = 1.47$ nH for the lumped-element equivalent circuit.

3. FABRICATION OF DUAL-BAND EVANESCENT-MODE GAP-COUPLED SIW BPF

Figure 5 schematically depicts the structure of the fabricated dual-band evanescent-mode BPF. The main resonator is coupled to the I/O ports with four open-circuited stubs. The filter is designed and fabricated on a single-layer Rogers RO4003C with a dielectric constant of 3.55 and thickness of 1.524 mm.

According to the operating principle of the structure in Section 2, the three sub-section SIWs can be modeled with three parallel LC circuits whose lumped-element components can be calculated by the cut-off frequency of the structure.
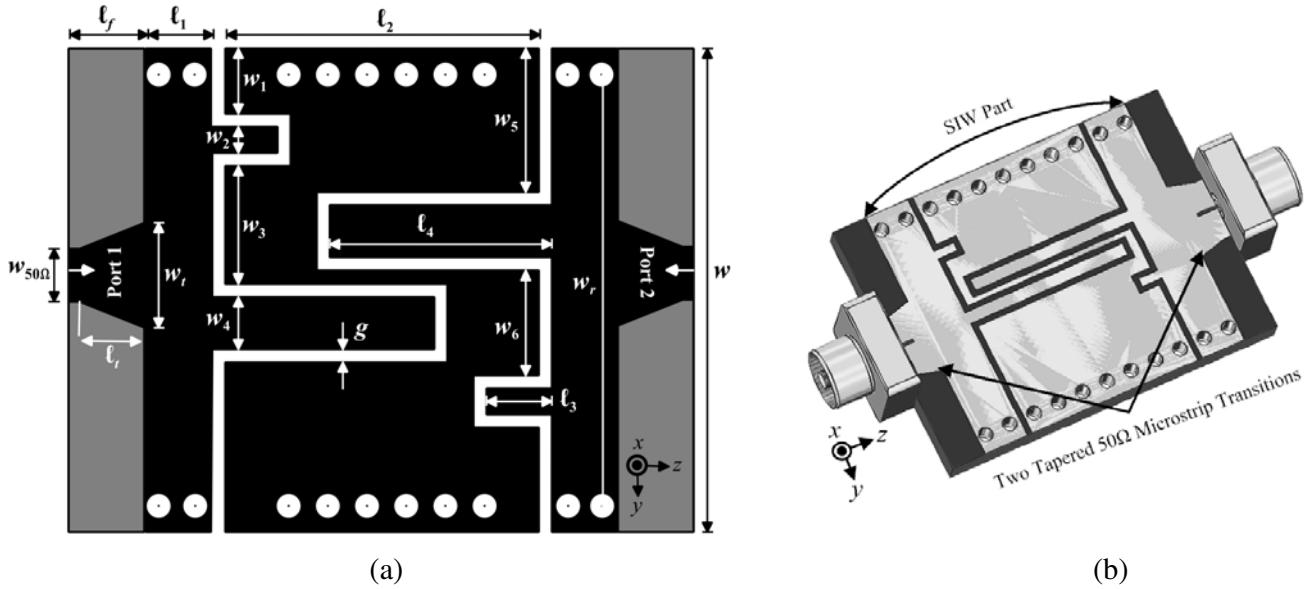
Figure 5. (a) Top view and (b) 3D diagram of the presented dual-band BPF with its critical dimensions. Two tapered $50\,\Omega$ microstrip lines are employed to feed the device.
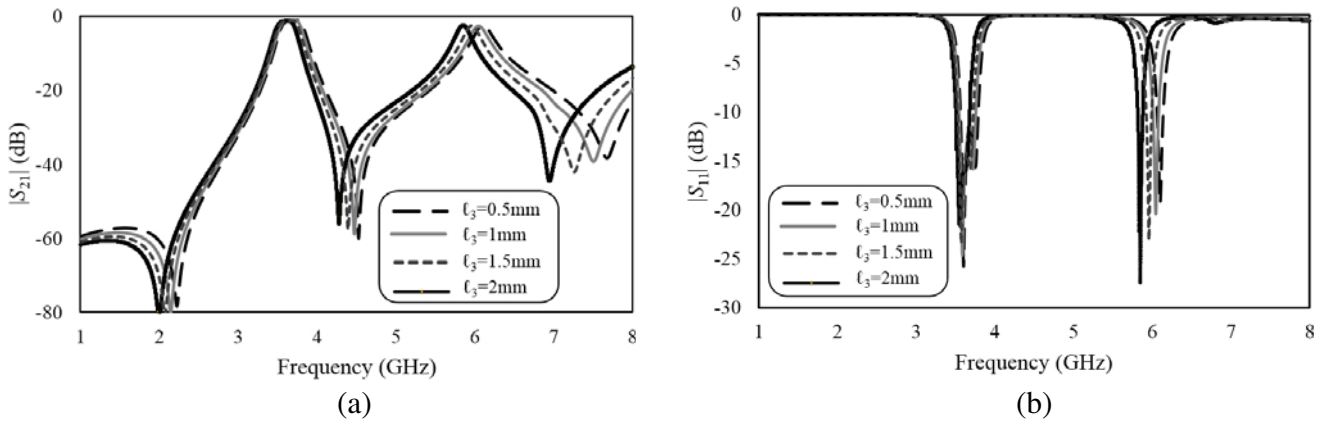

Figure 6. EM-simulated behavior of the proposed capacitively-coupled SIW-based BPF for four different values of $\ell_3 = 0.5\,\text{mm}$ ($f_{02} = 6.1\,\text{GHz}$, $IL = 2.51\,\text{dB}$, $RL = 19.3\,\text{dB}$, and $\text{FBW}_{3\,\text{dB}} = 3.77\%$), $\ell_3 = 1\,\text{mm}$ ($f_{02} = 6\,\text{GHz}$, $IL = 2.72\,\text{dB}$, $RL = 20.4\,\text{dB}$, and $\text{FBW}_{3\,\text{dB}} = 3.83\%$), $\ell_3 = 1.5\,\text{mm}$ ($f_{02} = 5.96\,\text{GHz}$, $IL = 2.73\,\text{dB}$, $RL = 23.1\,\text{dB}$, and $\text{FBW}_{3\,\text{dB}} = 3.52\%$), and $\ell_3 = 2\,\text{mm}$ ($f_{02} = 5.84\,\text{GHz}$, $IL = 2.5\,\text{dB}$, $RL = 27.5\,\text{dB}$, and $\text{FBW}_{3\,\text{dB}} = 3.25\%$). (a) $|S_{21}|$ and (b) $|S_{11}|$.

The two series LC circuits of the four open-circuited subs in the propagation direction (e.g., $L_{p1,2}$-$C_{p1,2}$) model the frequencies of the evanescent-mode TPs while their equivalent LC circuits in the transverse direction (e.g., $L_{z1,2}$-$C_{z1,2}$) stand for the frequencies of the TZs. Fig. 6 shows the EM-simulated S-parameters of the proposed capacitively-coupled SIW. The frequency of the second evanescent-mode TP accompanied by three TZs frequencies can be tuned by changing the length of the two shorter open-circuited stubs with the least impact on the resonance frequency of the first evanescent-mode TP.

Figure 7 gives a comparison between EM-simulated scattering parameters with those of the measured result ones and a digital photo of the fabricated dual-band BPF presented in Fig. 5. The measured results confirm that the structure realizes a dual-band evanescent-mode BPF at center frequencies of $f_{01} = 3.7\,\text{GHz}$ and $f_{02} = 5.96\,\text{GHz}$ which are below the cut-off frequency of $f_c = 6.5\,\text{GHz}$
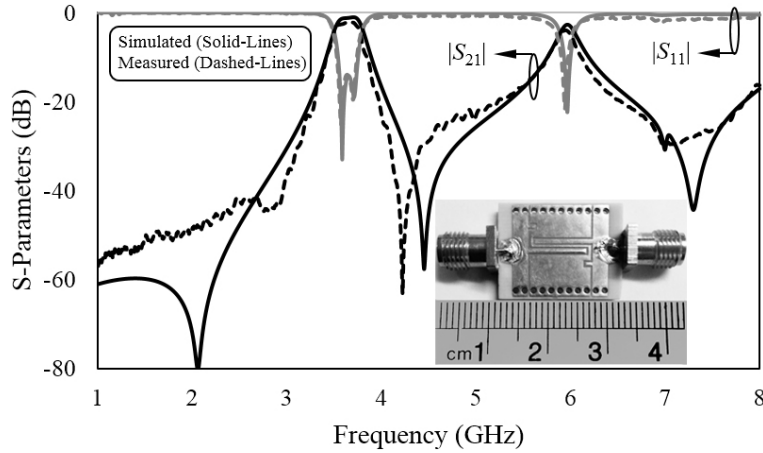
Figure 7. Comparison between EM-simulated S-Parameters (Finite Element Method, Ansys HFSS) and those of the measured for the developed BPF with optimized parameters of $\ell_1 = 2.6$, $\ell_2 = 10.2$, $\ell_3 = 1.2$, $\ell_4 = 9.7$, $w_1 = 3$, $w_2 = 0.5$, $w_3 = 2.8$, $w_4 = 0.7$, $w_5 = 5.3$, $w_6 = 2.5$, $w_r = 13$, $g = 0.3$, $\ell_f = 2$, $\ell_t = 1.5$, $w_{50\Omega} = 3.6$, and $w_t = 4.4$, all in mm. A photograph of the fabricated filter can be seen.

with the 3 dB-fractional bandwidths of $\text{FBW}_1 = 8.1\%$ and $\text{FBW}_2 = 3.52\%$, respectively.

The return losses are better than 33 dB and 22 dB while the insertion losses are less than 1 dB and 2.73 dB for the first and second frequency bands, respectively.

Table 1 compares the performances of the proposed dual-band evanescent-mode BPF with those of conventional counterparts in terms of IL, FBW, dimensions, etc. In comparison to the dual-band evanescent-mode BPFs in [7] and [8], the new filter, not only reduces the number of the substrate's layer from two to single one (complexity reduction), it also reduces the insertion loss with a trade-off between the insertion losses of the two passbands. Moreover, the proposed filter demonstrates a lower insertion loss compared to that of the filter developed in [11]. As can be seen from this table, in some references, e.g., [7] and [8], the SIW structure has been implemented on multi-layer substrate to realize dual-band BPF. While our proposed device is presented a dual-band BPF on just one layer substrate which reduce the fabrication cost compared to that of the multi-layer ones. It is also clear that the insertion loss has an inverse relation to the bandwidth. In other words, smaller bandwidths have larger insertion losses and vice versa. Therefore, there is a trade-off between the insertion loss and the bandwidth. For instance, the lower-band of this fabricated BPF has FBW of 8.1% and insertion loss of 1 dB. On the other hand, the upper-band has 3.5% and 2.7 dB of FBW and insertion loss, respectively. This structure clarifies that since the upper-band has a smaller bandwidth in contrast to lower-band, its insertion loss is greater than that of the lower-band one.

Table 1. Comparison of the performances of the proposed devise with those of the others state of the art dual-band SIW BPF ones.

BPF	Technology	f_0 (GHz)	IL (dB)	3 dB-FBW (%)	Dim. ($\lambda \times \lambda$)
[7]	Multi-Layer	1.5, 3	1, 4.6	6.6, 3.3	0.36×0.33
[8]	Multi-Layer	1.9, 3.76	2.3, 2	5.4, 2.8	0.16×0.16
[10]	Single-Layer	2.4, 5.2	0.8, 1	8.6, 6.1	0.67×0.3
[11]	Single-Layer	2.4, 5.2	3.6, 3.1	5.8, 6.4	0.15×0.16
This work	Single-Layer	3.7, 5.96	1, 2.73	8.1, 3.52	0.35×0.37

4. CONCLUSIONS

Gap-coupled excitation has been used to demonstrate the multiple transmission poles and zeros below the cut-off frequency of the SIW. A single-layer dual-band evanescent-mode SIW-based BPF has been designed and fabricated using gap-coupled excitation technique. The structure is reported to realize two independent evanescent-mode poles on a single-layer SIW which reduces the size and complexity of the structure compared to those of the recent multi-layer evanescent-mode structures. The EM behavior of the structure has been modeled with lumped-element equivalent circuit. A compact single-layer dual-band SIW filter has been fabricated to verify the capability of the proposed design method.

REFERENCES

1. Punitha, L., S. P. Sugumar, and P. H. Rao, "Analysis of RF transceiver for 5G applications," *Asia-Pacific Radio Sci. Conf.*, Mar. 2019.

2. Amari, S., U. Rosenberg, and J. Bornemann, "Adaptive synthesis and design of resonator filters with source/load-multiresonator coupling," *IEEE Trans. Microw. Theory Tech.*, Vol. 50, No. 8, 1969–1978, Aug. 2002.

3. Xu, F. and K. Wu, "Guided-wave and leakage characteristics of substrate integrated waveguide," *IEEE Trans. Microw. Theory Tech.*, Vol. 53, No. 1, 66–73, Jan. 2005.

4. Sirci, S., et al., "Design and multi-physics analysis of direct and cross-coupled SIW combline filters using electric and magnetic couplings," *IEEE Trans. Microw. Theory Tech.*, Vol. 63, No. 12, 4341–4354, Dec. 2015.

5. Dong, Y. D., T. Yang, and T. Itoh, "Substrate integrated waveguide loaded by complementary split-ring resonators and its applications to miniaturized waveguide filters," *IEEE Trans. Microw. Theory Tech.*, Vol. 57, No. 9, 2211–2223, Sep. 2009.

6. Nosrati, M., Z. Abbasi, and M. Daneshmand, "Single-layer substrate-integrated waveguide evanescent-mode filter," *IEEE Microw. Wirel. Components Lett.*, Vol. 28, No. 12, 1107–1109, Dec. 2018.

7. Nosrati, M. and M. Daneshmand, "Substrate integrated waveguide L-shaped iris for realization of transmission zero and evanescent-mode pole," *IEEE Trans. Microw. Theory Tech.*, Vol. 65, No. 7, 2310–2320, Jul. 2017.

8. Nosrati, M. and M. Daneshmand, "Gap-coupled excitation for evanescent-mode substrate integrated waveguide filters," *IEEE Trans. Microw. Theory Tech.*, Vol. 66, No. 6, 3028–3035, Jun. 2018.

9. Dong, Y. and T. Itoh, "Miniaturized dual-band substrate integrated waveguide filters using complementary split-ring resonators," *IEEE MTT-S Int. Microw. Symp. Dig.*, 1–4, Jun. 2011.

10. Wu, L.-S., J.-F. Mao, W.-Y. Yin, and Y.-X. Guo, "A dual-band filter using Stepped-Impedance Resonator (SIR) embedded into Substrate Integrated Waveguide (SIW)," *Proc. IEEE Elect. Design Adv. Packag. Syst. Symp.*, 1–4, Dec. 2010.

11. Xu, S., K. Ma, F. Meng, and K. S. Yeo, "Novel defected ground structure and two-side loading scheme for miniaturized dual-band SIW bandpass filter designs," *IEEE Microw. Wireless Compon. Lett.*, Vol. 25, No. 4, 217–219, Apr. 2015.